

Si_{1-x}Ge_x Single Crystals Grown by the Czochralski Method: Defects and Electrical Properties

T.S. ARGUNOVA^{a,b}, J.H. JE^{b,*}, L.S. KOSTINA^a, A.V. ROZHKOV^a AND I.V. GREKHOV^a

^aIoffe Physical-Technical Institute, RAS, Polytekhnicheskaya st. 26, 194021 St. Petersburg, Russia

^bX-ray Imaging Center, Department of Materials Science and Engineering, Pohang University of Science and Technology, San 31 Hyoja-dong, Namku, 790-784 Pohang, Republic of Korea

Defects in Si_{1-x}Ge_x single crystals (2–8.5 at.% Ge) grown by the Czochralski method are investigated by synchrotron white beam topography and phase contrast imaging techniques. As the Ge concentration increases, dislocation structure evolves from individual dislocations to slip bands and sub-grain boundaries. We discuss the effect of dislocations on the electrical characteristics such as resistivity ρ_v , the Hall hole mobility μ_p and carrier lifetime τ_e . Diodes are fabricated by bonding *p*-Si_{1-x}Ge_x to *n*-Si wafers to investigate *I*-*V* characteristics and reverse recovery process. *I*-*V* characteristics are not deteriorated in spite of a five times decrease in τ_e with Ge concentration. A small reverse recovery time (determined by the accumulated charge) can be achieved for an optimised preset Ge concentration.

DOI: [10.12693/APhysPolA.124.239](https://doi.org/10.12693/APhysPolA.124.239)

PACS: 61.72.Ff, 61.72.Lk, 72.15.Eb

1. Introduction

Si_{1-x}Ge_x (SiGe) solid solutions are presently used to fabricate high-power high-speed bipolar transistors (HBTs) [1], *p-i-n* diodes [2], field-effect transistors (FETs) [3], and integrated circuits for operation at ultra-high frequencies. SiGe layers are grown on silicon substrates by epitaxial growth technologies such as ultra-high vacuum chemical vapor deposition or molecular beam epitaxy [1, 3]. SiGe single crystals are becoming available as well [4–6], though their commercial production is not set yet.

In bipolar transistors, a SiGe base with a graded SiGe profile is used [1]. The increase in Ge content brings about high lattice mismatch between SiGe layer and Si substrate, giving rise to high elastic stress. By the relaxation of the stress, misfit and threading dislocations are generated, which affect device performance and production yield.

In FET structures, a tensile strained silicon channel is formed on a relaxed SiGe buffer layer by epitaxial growth [3]. The carrier mobility in the channel is then significantly enhanced by a factor of 3 to 5, comparing to bulk silicon, due to reduced effective masses of carriers and weak intervalley scattering, which cause high frequency characteristics of FET transistors.

Specifically, to fabricate tensile strained silicon channel, a SiGe buffer layer is first grown on Si wafer by gradually increasing Ge content (15–30% Ge) until the strain relaxes by the generation of high density of misfit and threading dislocations. Then the continued SiGe growth

results in the formation of a relaxed SiGe layer with a relatively low (10^5 to 10^7 cm⁻²) threading dislocation density on which a strained Si channel is grown [1, 3]. The foremost critical challenge in the FET technology is the control of dislocation defects in the epitaxial layers. The method includes preliminary fabrication of SiGe layers on Si substrates using epitaxial technology.

In this review, we suggest an alternative approach, direct binding of SiGe and Si single-crystal wafers, to form the relaxed Si_{1-x}Ge_x/Si compositions with satisfactory structural and electrical characteristics [7–9]. Misfit dislocations in such structures are localized in a thin layer near the interface where strain relaxation occurs without generating threading dislocations.

Structural defects in SiGe bulk affect the electrical properties of the bonded structures. We studied the evolution of dislocations in SiGe single crystals by the increase in Ge concentration. Good quality single crystals up to 50 mm in diameter with Ge concentrations of up to 15 at.% were produced with the Czochralski (Cz) technique [4]. The main difficulty in Cz growth is caused by fluctuations of the crystallization rate at the solid-liquid interface. Together with the effect of a high segregation coefficient of germanium in silicon and the risk of constitutional supercooling, fluctuations lead to the formation of Ge striations [10]. Striations then induce strain [11] and, depending on Ge content, may cause plastic deformation in the lattice [12].

The electrical parameters of bulk Si_{1-x}Ge_x were previously investigated [4, 13, 14], but multiplication of dislocations with Ge content or any correlation between the structure and the properties are largely unexplored. We discuss the perfection of Cz-grown Si_{1-x}Ge_x single crystals ($0.02 < x \leq 0.085$) and compare the structural quality with the electrical resistance and the carrier lifetime measured in the pre-studied samples [15, 8]. We also an-

*corresponding author; e-mail: jhje@postech.ac.kr

alyze current–voltage characteristics and reverse recovery processes from the bonded diodes $p\text{-Si}_{1-x}\text{Ge}_x/n\text{-Si}$ [7, 16].

2. Samples and techniques

$\text{Si}_{1-x}\text{Ge}_x$ single crystals were grown by the Czochralski method [4]. The germanium concentration changed from 2 to 8.5 at.%. Crystals (with n - or p -type conductivity) were lightly doped with phosphorus or boron to a concentration of approximately 10^{15} cm^{-3} . The oxygen content was at a level of 10^{17} cm^{-3} . The growth was performed in the $\langle 111 \rangle$ ($0.02 < x < 0.08$) and $\langle 100 \rangle$ ($x = 0.085$) directions. The samples were cut perpendicularly to the growth direction and polished at both sides to a thickness of 0.4 mm.

To fabricate $p\text{-SiGe}/n\text{-Si}$ heterostructures, mirror-polished $p\text{-SiGe}$ wafers were bonded to dislocation-free n -type Si wafers of the same orientation. Prior to bonding, an artificial relief in the form of an orthogonal net of grooves was photolithographically prepared on the Si wafer surfaces [9]. After RCA cleaning, the wafers were joined under the deionized water surface, spin-dried and heated at 95°C for 4 h. Bonding annealing was performed in air in two steps: at 1000°C (1 h) and 1150°C (2 h).

Structural defects in the SiGe bulk and at the SiGe/Si interfaces were investigated by X-ray topography combined with phase contrast imaging [8, 15, 17]. The experiments were performed on the 7B2 X-ray microscopy beamline of the Pohang Light Source, which is third-generation synchrotron radiation (SR) source, in Pohang, Republic of Korea. A bending magnet was used to offer an effective source size of $160\ \mu\text{m} \times 60\ \mu\text{m}$ ($H \times V$) at a distance of 34 m from the sample. The initial spectrum showed a monotonic decrease in the range from 6 to 40 keV. There were no optical elements between the source and sample. Partially coherent imaging with a white beam was feasible due to the fact that the effective spectrum was shaped with a maximum by the absorption in a Be window and in the sample [18].

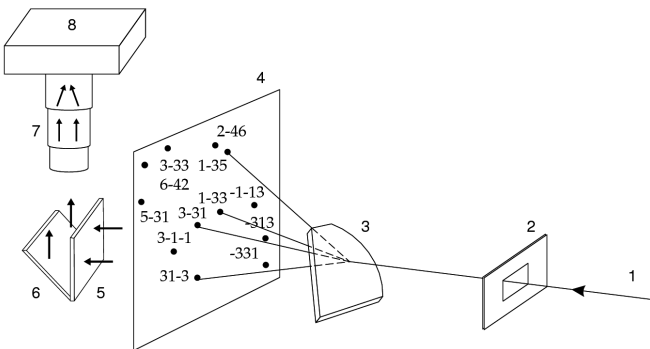


Fig. 1. Scheme for obtaining Laue-diffraction and phase-contrast images on-line. 1 — polychromatic beam, 2 — slit, 3 — sample, 4 — film, 5 — scintillator, 6 — mirror, 7 — objective, 8 — CCD.

Images were obtained in several ways (Fig. 1). Phase-contrast images were always recorded on the detector by transforming X-rays into visible light using a $200\ \mu\text{m}$ thick CdWO_4 scintillator. The CCD array had $1600\text{ pixels} \times 1200\text{ pixels}$ and a sensitivity of 12 bit. Images were magnified before recording with an objective lens. Depending on the objective magnification, the field of view could be changed from several millimeters to several dozens of micrometers. The effective pixel size was $0.19\ \mu\text{m}$ for high-resolution images. The scintillator–sample distance was chosen in the range of 6–10 cm.

Topographs in the Laue or Bragg geometries were recorded using either a photographic film or the detector. A high-resolution KODAK SR-45 film was placed at a distance of 8–12 cm behind the sample. The beam size on the sample was $10\text{ mm} \times 10\text{ mm}$. Topographs were magnified in an optical microscope. When recording on the detector, the field of view did not exceed $1.5\text{ mm} \times 1.5\text{ mm}$ [19].

When polychromatic radiation is allowed to fall on a single crystal, several diffracted beams are recorded simultaneously. Topographs in various reflections were used to determine the dislocation Burgers vectors \mathbf{b} according to the visibility criteria [20].

The electrical resistivity, the carrier lifetime, the current–voltage (I – V) characteristics, and the reverse recovery process wave forms were measured. The germanium distribution was investigated by means of energy dispersive X-ray (EDX) analysis on a JEOL JSM-6330F FESEM system.

3. Investigation of lattice defects in SiGe crystals

We performed a comparative study of defects in $\text{Si}_{1-x}\text{Ge}_x$ crystals with $0.02 < x \leq 0.085$. As a rule, dislocations were not observed in the range $x \leq 0.05$, where Ge striations were the main structural defects. Dislocations appeared for high Ge concentrations ($x > 0.05$). Figure 2 represents white beam topographs of $\text{Si}_{0.946}\text{Ge}_{0.054}$ (111) taken from a region between the center and the periphery of the wafer. The 200 (a) and 020 (b) reflections were feasible because of twinning and the change in the growth axis from $\langle 111 \rangle$ to $\langle 115 \rangle$. One can see variations of the dislocation density in the 200 and the 020 topographs. In particular, the dislocations that strongly stand out in (b) but disappear in (a) are presumably produced by a Frank–Read source [21], as can be seen in the inset to (b) for a Frank–Read source nearby but outside the scope of the image. The dislocations were invisible in the $3\bar{1}\bar{1}$ topograph (data not shown), indicating that they belong to the (111), $[01\bar{1}]$ slip system. The other type of dislocations lying in the (111) slip plane is seen in the upper right-hand corner of (a) but invisible in (b), proving that their Burgers vectors are parallel to $[10\bar{1}]$. The dislocation density N_d in each slip system was remarkably low, less than $\approx 10^2\text{ cm}^{-2}$ for $x = 0.054$.

As Ge concentration increased to 6.4 at.%, the SiGe crystals showed a larger number of dislocation sources

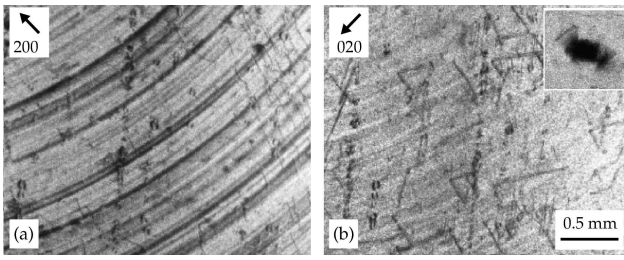


Fig. 2. White beam topographs for $Si_{0.946}Ge_{0.054}$ crystal showing dislocations belonging to two slip systems, each with the density $\approx 10^2 \text{ cm}^{-2}$. Inset to (b) displays the image of a Frank-Read source responsible for the multiplication of dislocations in (b). The variations in the dislocation visibility between (a) and (b) are explained in the text.

and their higher activities. The locations of these sources were related to Ge segregation bands, like in Fig. 3, where a Frank-Read source and segregation bands are marked with numbers 1 and 2, respectively. In Fig. 3, dislocation loops gliding in the (111) slip plane are seen, which stand bright in the reflection $3\bar{1}\bar{1}$ and are indistinguishable in the reflection $\bar{1}\bar{1}3$. The comparison of the loops images in (a) and (b) allows one to assign their Burgers vector to $[\bar{1}10]$. Individual dislocations were still resolvable; however, when dislocations from different slip systems started to overlap (data not shown), the dislocation density increased to $N_d = 10^3 - 10^4 \text{ cm}^{-2}$. In addition, there were dislocation slip bands (3) which propagated from the ingot periphery as seen in Fig. 3b.

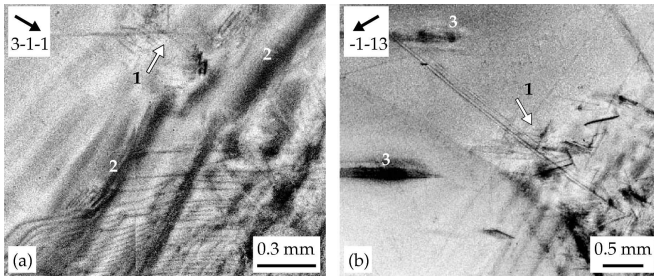


Fig. 3. Topographs in different reflections obtained for the $Si_{0.93}Ge_{0.07}$ (111) crystal. 1 — Frank-Read source, 2 — Ge segregation bands, 3 — slip bands propagating from the ingot periphery.

Ge segregation bands were observed to become fragmentary in shape. Fragmentation increased with germanium content. Each fragment, a region of high Ge concentration, can be considered as possessing an intrinsic strain caused by a lattice misfit and a difference in the coefficients of thermal expansion between the fragment and the surrounding material. In the thermoelastic stress field, dislocations multiplied according to the Frank-Read mechanism [21]. With an increase in the germanium concentration in the melt, germanium evaporation from the melt surface and its deposition on the

crystal surface led to the formation of misfit dislocations, which slipped from the periphery into the bulk forming slip bands.

As Ge concentration further increased above 8 at.%, plastic deformation evolved. Topographs of $Si_{0.915}Ge_{0.085}$ wafer are shown in Fig. 4. Individual dislocations are no longer resolved due to the overlapping of strain fields; instead one can see low- and high-angle subgrain boundaries. Based on the overlapping of strain fields, the dislocation density between boundaries was inferred as $N_d \approx 10^5 - 10^6 \text{ cm}^{-2}$, which is just higher than the limit of spatial resolution achievable in the Bragg diffraction geometry [20].

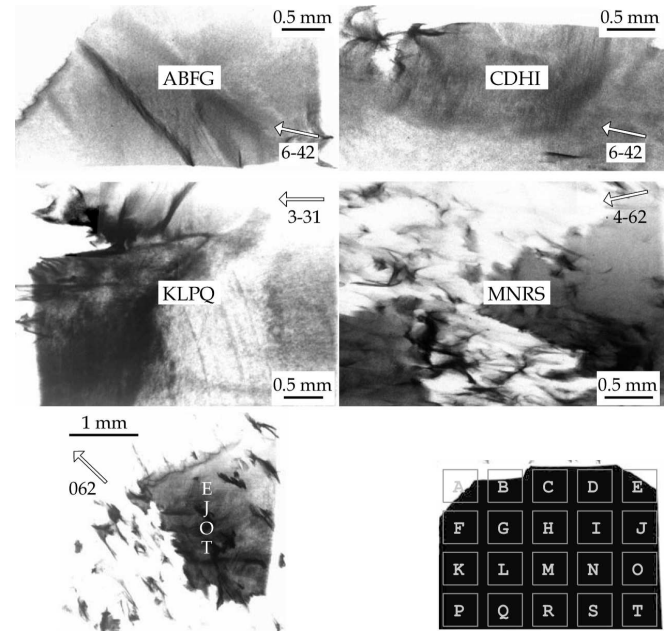


Fig. 4. Topographs for the $Si_{0.915}Ge_{0.085}$ sample. The letters A, B, C, . . . , and T on the sample contour indicate the areas where the Ge content and electrical resistance were measured.

The specimens with $x = 0.085$ were used to investigate a correlation between microstructure, Ge distribution, and electric resistance. Defect distribution maps were provided (Fig. 4). One can see that the defect distribution, which is more uniform in the upper and left parts of the wafer (ABFG, CDHI, and KLPQ areas), becomes significantly nonuniform in the bottom (MNRS) and, especially, in the right (EJOT) parts, where high-angle grain boundaries arise with the decrease in the grain size. Here the letters A, B, C . . . indicate the squares of the sample contour, as illustrated in the right bottom corner of Fig. 4.

The Ge distribution over each sample area was measured by EDX. The sheet resistance R was determined by the four-point probe method, and the specific volume resistivity ρ_v was calculated from $R: \rho_v = Rt$, where t is the sample thickness. The mean values, which were obtained by measuring both the composition and sheet resistance, are listed in Table.

TABLE

Distribution of the Ge content and electrical resistance over the area of the $\text{Si}_{0.915}\text{Ge}_{0.085}$ sample.

Areas A–J	A	B	C	D	E	F	G	H	I	J
Ge [at.%]	9.0	8.7	8.8	8.6	8.7	8.7	8.7	8.7	8.8	7.8
R [Ω]	–	88	–	111	–	–	76	–	71	–
Areas K–T	K	L	M	N	O	P	Q	R	S	T
Ge [at.%]	8.9	8.8	8.6	8.6	8.5	8.8	8.5	8.6	8.7	8.9
R [Ω]	–	75	–	73	–	113	84	90	91	94

Comparison of Fig. 4 with Table shows that the composition distribution over the sample area does not correlate with the dislocation density. The spread of the values listed in Table is within the error range of the EDX measurement. The deviations of the R values from the mean over the sample are small and within $\pm 5\%$. The volume resistivity ρ_v , calculated for the most distorted *MNRS* and *EJOT* regions, is $\rho_{v(1)} = 2.44 \Omega \text{ cm}$. At the same time, for the relatively homogeneous *ABFG* region, it is $\rho_{v(2)} = 2.26 \Omega \text{ cm}$. This small change in ρ_v can be hardly correlated with the structure.

4. Electrical properties of heterojunctions $\text{Si}_{1-x}\text{Ge}_x/\text{Si}$ ($0.02 < x \leq 0.08$)

Heterodiodes were fabricated by the direct bonding of (111)-oriented *n*-type single crystal silicon wafers to *p*-type $\text{Si}_{1-x}\text{Ge}_x$ ($0.02 < x \leq 0.08$) wafers of the same orientation. The results of the electrical measurements showed that, as the germanium concentration N_{Ge} increased, the minority carrier lifetime decreased: the heterodiodes with a *p*- $\text{Si}_{1-x}\text{Ge}_x$ base containing $N_{\text{Ge}} = 2.5, 5.0,$ and $8.0 \text{ at.}\%$ were characterized by $\tau_e = 12, 8,$ and $2.5 \mu\text{s}$, respectively. This significant decrease in τ_e with Ge content can be explained by an increase in the density of structural defects in the $\text{Si}_{1-x}\text{Ge}_x$ base layers. The decrease in τ_e leads to a growth in the recombination component of the forward current flowing through the *p*–*n* junction as well as in the differential resistance of the *I*–*V* curve. The reverse voltages in all cases did not exceed 200 V; and the leakage current was small as $I_{\text{leak}} < 100 \mu\text{A}$ at 300 K [15].

The forward *I*–*V* characteristics were measured in the dc and pulse current modes at room temperature in the range of current densities from 1 mA/cm^2 to 200 A/cm^2 . The *I*–*V* curves were qualitatively similar to each other for $0.025 \leq x \leq 0.08$. In the initial region (for bias voltages of 0.03–0.12 V and currents of 5×10^{-8} – 8×10^{-6} A), the curves of all samples virtually coincided and exhibited the same exponential character with a nonideality factor of $\beta \approx 1.25$ [15]. This was indicative of a predominating diffusion current in the junction and a sufficiently weak influence of defects present at the bonding interface on the current flow. As the bias voltage increased further, the *I*–*V* curves began to deviate from the exponent. A decrease in the slope of the $I = f(V)$ curves at higher bias voltages (which was especially pronounced for the samples with a $\text{Si}_{0.85}\text{Ge}_{0.15}$ base, data not shown)

was related to both the current limitation by the serial resistance of the sample bulk and the insufficient modulation of the base resistance due to a short lifetime τ_e of minority carriers (electrons).

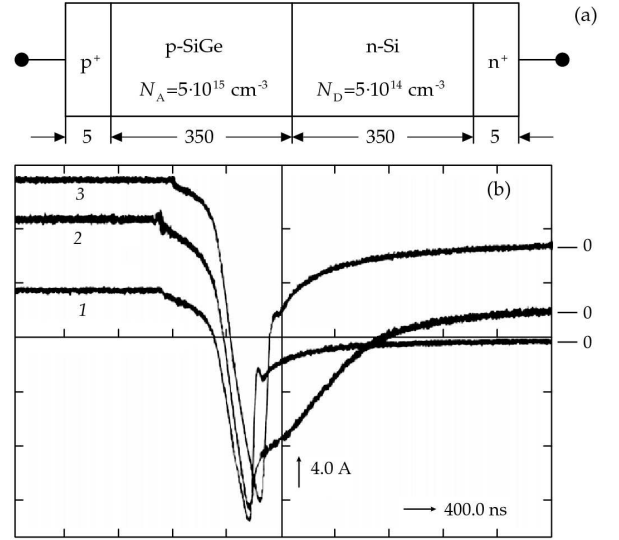


Fig. 5. Fast-recovery *n*-Si/*p*- $\text{Si}_{1-x}\text{Ge}_x$ heterodiode structures fabricated by direct bonding: (a) diagram of the diode (layer thicknesses are indicated in μm); (b) typical reverse recovery process wave forms measured upon bias voltage switching from forward to reverse for the samples with Ge content in the *p*-type layer $N_{\text{Ge}} = 7.6$ (1), 4.1 (2), and 5.3 at.% (3).

By means of surface grooved bonding technology we fabricated high power high voltage fast switched-off diodes with the switched current density up to 100 A/cm^2 and the voltage up to 350 V at leakage current less than $100 \mu\text{A}$. Such diodes represent an alternative to conventional silicon diodes made by impurities diffusion with subsequent proton irradiation. Figure 5a shows a schematic diagram of the bonded diode structure. Wave forms of the reverse recovery process measured at a forward current density of $\approx 60 \text{ A/cm}^2$ are displayed in Fig. 5b. As can be seen, the reverse recovery time of SiGe/Si heterodiodes decreases by almost an order of magnitude, from 800 to 100 ns, when the Ge content in the SiGe wafer increases from 4.1 to 7.6 at.%. During the passage of the electron component of the forward current, the charge accumulated in the *p*-type layer is determined by the minority carrier lifetime in this layer, which decreases with Ge content. This shows that the direct bonding technology makes it possible to fabricate *n*-Si/*p*-SiGe heterodiodes with small reverse recovery time (determined by the accumulated charge) when *n*-Si and *p*-SiGe wafers are selected for a preset Ge concentration with an optimal combination of structural and electrical parameters.

5. Conclusions

In the heteroepitaxial structures Si_{1-x}Ge_x/Si with Ge concentrations of ≥ 10 at.%, the critical thickness, i.e. the maximum thickness for pseudomorphic growth, is $t_c < 100$ nm and an excess of the thickness results in the threading dislocation densities exceeding 10^8 cm⁻². Unlike epitaxial growth, bonding of dissimilar materials allows one to avoid the formation of threading dislocations [22]. Moreover, in the surface-grooved wafer bonding, the grooves act as sinks for the dislocations during annealing [9] and reduce the concentration of deep level centers several times. The structural quality of bonded compositions is determined by the quality of bonding pairs, hence by the perfection of the SiGe bulk. We found that the increase in Ge concentration up to 8.5 at.% does not cause the multiplication of dislocations over the density $N_d \approx 10^6$ cm⁻².

The increase in the density of structural defects leads to a growth in the recombination component of the forward current passing in the *p-n* junction. However, for all samples with $N_{Ge} \leq 8$ at.%, the *I-V* curves of Si_{1-x}Ge_x/Si heterodiodes are satisfactory in the entire range of current densities (1 mA/cm²–200 A/cm²), which shows good prospects for using direct bonding technology in the formation of Si_{1-x}Ge_x/Si heterostructures.

Acknowledgments

This work was supported by the Creative Research Initiatives (Functional X-ray Imaging) of MEST/KOSEF of Korea. The authors are greatly indebted to N.V. Abrosimov from the Institute of Crystal Growth, Berlin, Germany, and Institute of Solid State Physics, RAS, Chernogolovka, Russia for making available the SiGe single-crystal samples.

References

- [1] D.L. Hareme, S.J. Koester, G. Freeman, P. Cottrel, K. Rim, G. Dehlinger, D. Ahlgren, J.S. Dunn, D. Greenberg, A. Joseph, F. Anderson, J.-S. Rieh, S.A.S.T. Onge, D. Coolbaugh, V. Ramachandran, J.D. Cressler, S. Subbanna, *Appl. Surf. Sci.* **224**, 9 (2004).
- [2] D. Hirose, Y. Souda, K. Nakano, S. Goya, T. Nishimori, S. Okumura, *IEEE Trans. Electron. Dev.* **48**, 2417 (2001).
- [3] K. Rim, R. Anderson, D. Boyd, F. Cardone, K. Chan, H. Chen, S. Christansen, J. Chu, K. Jenkins, T. Karnarsky, S. Koester, B.H. Lee, K. Lee, V. Mazzeo, A. Mocuta, D. Mocuta, P.M. Mooney, P. Oldiges, J. Ott, P. Ronsheim, R. Roy, A. Steegen, M. Yang, H. Zhu, M. Jeong, H.-S.P. Wong, *Solid-State Electron.* **47**, 1133 (2003).
- [4] N.V. Abrosimov, S.N. Rossolenko, V. Alex, A. Gerhardt, W. Schröder, *J. Cryst. Growth* **166**, 657 (1996).
- [5] K. Nakajima, Sh. Kodama, S. Miyashita, G. Sazaki, S. Hiyamizu, *J. Cryst. Growth* **205**, 270 (1999).
- [6] M.S. Saidov, A. Yusupov, R.S. Umerov, *J. Cryst. Growth* **52**, 514 (1981).
- [7] I.V. Grekhov, E.I. Belyakova, L.S. Kostina, A.V. Rozhkov, Sh.A. Yusupova, L.M. Sorokin, T.S. Argunova, N.V. Abrosimov, N.A. Matchanov, J.H. Je, *Tech. Phys. Lett.* **34**, 1027 (2008).
- [8] T.S. Argunova, E.I. Belyakova, I.V. Grekhov, A.G. Zabrodskii, L.S. Kostina, L.M. Sorokin, N.M. Shmidt, J.M. Yi, J.W. Jung, J.H. Je, N.V. Abrosimov, *Semiconductors* **41**, 679 (2007).
- [9] E.D. Kim, N.K. Kim, S.C. Kim, I.V. Grekhov, T.S. Argunova, L.S. Kostina, T.V. Kudryavtzeva, *Electron. Lett.* **31**, 2047 (1995).
- [10] O.V. Smirnova, V.V. Kalaev, Yu.N. Makarov, N.V. Abrosimov, H. Riemann, *J. Cryst. Growth* **287**, 281 (2006).
- [11] K. Wieteska, W. Wierzchowski, W. Graeff, M. Lefeld-Sonowska, M. Regulaska, *J. Phys. D, Appl. Phys.* **36**, A133 (2003).
- [12] L. Sorokin, T. Argunova, N. Abrosimov, M. Gutkin, A. Zabrodski, L. Kostina, J.-W. Jung, J.-H. Je, *Tech. Phys. Lett.* **33**, 512 (2007).
- [13] P. Gaworzewski, K. Tittelbach-Helmrich, U. Penner, N. Abrosimov, *J. Appl. Phys.* **83**, 5258 (1998).
- [14] A. Ulyashin, N. Abrosimov, A. Bentzenc, A. Suphellen, E. Sauard, B. Svensson, *Mater. Sci. Semicond. Process.* **9**, 772 (2006).
- [15] T.S. Argunova, J.-W. Jung, J.-H. Je, N.V. Abrosimov, I.V. Grekhov, L.S. Kostina, A.V. Rozhkov, L.M. Sorokin, A.G. Zabrodskii, *J. Phys. D, Appl. Phys.* **42**, 085404 (2009).
- [16] I.V. Grekhov, E.I. Belyakova, L.S. Kostina, A.V. Rozhkov, T.S. Argunova, G.A. Oganessian, *Tech. Phys. Lett.* **37**, 632 (2011).
- [17] T.S. Argunova, A.G. Zabrodskii, L.M. Sorokin, N.V. Abrosimov, J.H. Je, *Crystallogr. Rep.* **56**, 811 (2011).
- [18] V.G. Kohn, T.S. Argunova, J.H. Je, *Appl. Phys. Lett.* **91**, 171901 (2007).
- [19] J.M. Yi, S.K. Seol, J.H. Je, T.S. Argunova, Y. Hwu, W.-L. Tsai, *Nucl. Instrum. Methods Phys. Res. A* **551**, 152 (2005).
- [20] D.K. Bowen, B.K. Tanner, *High Resolution X-ray Diffractometry and Topography*, Taylor and Francis, London 1998.
- [21] J.P. Hirth, J. Lothe, *Theory of Dislocations*, 2nd ed., Wiley, New York 1982.
- [22] A. Plöchl, G. Kräuter, *Mater. Sci. Eng. R* **25**, 1 (1999).